https://rbgeomorfologia.org.br/
*ISSN 2236-5664*

**Revista Brasileira de Geomorfologia**

v. 27, nº 1 (2025)

https://dx.doi.org/10.20502/rbg.v27i1.2714

*Research Paper*

# Shallow landslide hazard assessment in the Camburi river catchment, São Sebastião municipality – SP

## *Avaliação do perigo a escorregamentos rasos na bacia do rio Camburi, município de São Sebastião – SP*

**Sofia Bonfogo Cavichioli[1]; Marina Tamaki de Oliveira Sugiyama[2]; José Eduardo Bonini[3]; Tiago Damas Martins[4]; Bianca Carvalho Vieira[5]**

[1] Universidade de São Paulo, Departamento de Geografia, São Paulo, Brasil. sofiabcavichioli@usp.br.
ORCID: https://orcid.org/0009-0003-7926-6329

[2] Universidade de São Paulo, Departamento de Geografia, São Paulo, Brasil. marinatamaki@usp.br
ORCID: https://orcid.org/0000-0001-9627-2403

[3] Universidade de São Paulo, Departamento de Geografia, São Paulo, Brasil. jose.bonini@usp.br
ORCID: https://orcid.org/0000-0001-6047-0141

[4] Universidade Federal de São Paulo, Departamento de Geografia, São Paulo, Brasil. td.martins@unifesp.br
ORCID: https://orcid.org/0000-0002-1213-1441

[5] Universidade de São Paulo, Departamento de Geografia, São Paulo, Brasil. biancacv@usp.br
ORCID: https://orcid.org/0000-0001-7060-2830

Received: 09/06/2025; Accepted: 09/12/2025; Published: 15/12/2025.

**Abstract:** In February 2023, the São Sebastião municipality (São Paulo State, Brazil) was hit by an extreme rainfall event that triggered hundreds of shallow landslides on the Serra do Mar slopes, outlining the necessity for detailed landslide hazard cartography. This research aims to quantitatively assess the hazard posed by landslides to the exposed elements of the Camburi river basin, located in São Sebastião. Susceptibility was evaluated through the SHALSTAB model, achieving good results (sensitivity = 0,865, specificity = 0,457, and F1-score = 0,720), allowing to identify unstable areas associated with rainfall thresholds up to 50mm/day. Hazard was assessed using the Gravitational Process Path (GPP) model, with reasonable accuracy for the final coupled model (ROC-AUC = 0,720). Approximatively 69% of the basin was classified as low and very low hazard areas, with 8% associated with high and very high hazard zones. We were able to identify buildings located in areas classified as both unstable and in the landslide runout zones, highlighting the coupling between irregular land tenure and geomorphological risk.

**Keywords:** SHALTAB; Gravitational Process Path; Serra do Mar.

**Resumo:** Em fevereiro de 2023, o município de São Sebastião (SP) foi fortemente afetado por um evento extremo de precipitação que deflagrou centenas de escorregamentos rasos nas vertentes da Serra do Mar, evidenciando a necessidade de cartografias de perigo em maior detalhe. O objetivo desta pesquisa foi avaliar quantitativamente o perigo aos elementos expostos na bacia do rio Camburi, no município de São Sebastião. A suscetibilidade foi analisada através do modelo SHALSTAB, com bom desempenho (sensitividade 0,865; especificidade 0,457; escore F1 0,720), identificando áreas instáveis associadas, sobretudo, a limiares de precipitação até os 50mm/dia. O perigo foi estimado a partir do *Gravitational Process Path* (GPP), com desempenho razoável para o modelo com ambas as suas componentes acopladas (AAC-ROC =0,720). Assim, 69% da bacia possui perigo baixo ou muito baixo, e 8%, alto ou muito alto. Foram identificadas edificações em setores instáveis e em trajetórias de escorregamentos, evidenciando sobreposição entre ocupação irregular e risco geomorfológico.

**Palavras-chave:** SHALSTAB; Gravitational Process Path; Serra do Mar.

## 1. Introduction

Mass movements are natural processes that can cause significant impacts, leading to economic, social, and environmental damage. The trend of increasing fatalities over the past century primarily reflects the expansion of human occupation in areas prone to these processes (Gómez; García; Aristizábal, 2023; Alcántara-Ayala, 2025). Although Brazil ranks twentieth in terms of the density of mass movements per square kilometer, it ranks eleventh in the global ranking when considering the number of deaths per million inhabitants (Gómez; García; Aristizábal, 2023). Considering the vast territorial extent of the country and the high population density in the most affected regions — such as the Serra do Mar, the Serra da Mantiqueira, and the Serra Geral — the number of fatalities becomes even more concerning.

In the Serra do Mar region, the existence of steep slopes with shallow soils, combined with prolonged rainfall and high total precipitation, leads to the frequent occurrence of mass movement events (Avelar et al., 2013; Bonini et al., 2021; Bonini; Vieira; Martins, 2022; Kanji; Cruz; Massad, 2008). Between 1928 and 2013, approximately 3,330 fatalities were reported in the Serra do Mar region due to mass movements, with about 43% of that total occurring between 2000 and 2013 alone (Vieira; Gramani, 2015). In February 2023, the municipalities of São Sebastião and Ilhabela, in the State of São Paulo, were severely affected by shallow landslides, debris flows, and floods, resulting in 46 fatalities, 1,686 displaced people, and 40 missing persons (Marengo et al., 2024), in addition to damage to infrastructure and tourism activities (Figure 1). Previous research shows that at least 585 landslides were triggered during this event (Bonini et al., 2025), a total rainfall of 626 mm was recorded in 24 hours. (Marengo et al., 2024).

Since 2014, the Brazilian Geological Survey (SGB-CPRM) and the Institute for Technological Research (IPT) have been working to map susceptibility to mass movements and hydrodynamic processes and to carry out risk zoning of Brazilian municipalities (Vieira et al., 2024). The landslide susceptibility maps developed by CPRM were produced using statistical methods, considering slope, curvature, and density of structural lineaments as conditioning factors (IPT; CPRM, 2014). The susceptibility mapping for the municipality of São Sebastião (CPRM, 2017), produced at a scale of 1:25,000, shows that approximately 53% of the municipality's area is in areas mapped as having medium to high susceptibility to shallow landslides, and these areas encompass approximately 4.5% of the municipality's urbanized area.

The analysis of natural susceptibility to shallow landslides represents a fundamental step in the assessment of risk scenarios, indicating a potential probability of spatial occurrence of the process in unaffected areas, but with similar physiographic conditions, based on different morphological and hydrological parameters (Corominas et al., 2013; Guzzetti et al., 1999). Among the different methods employed, physically-based models stand out, which rely on a deterministic approach, allowing the quantification of critical values from mathematical equations supported by a set of physical parameters. One of these models is SHALSTAB (*Shallow Landsliding Stability Model*), developed by Montgomery and Dietrich (1994), which has been widely adopted in the Serra do Mar region, producing positive results in terms of susceptibility linked to a precipitation threshold (Vieira; Ramos, 2015; Martins et al., 2016; Bonini et al., 2020).

However, to assess a risk scenario, based on natural susceptibility to the occurrence of the process, it is necessary to prepare hazard maps. Risk is understood as "the expected number of lives lost, people injured, damage to property and disruption of economic activities due to a harmful phenomenon, in a given area and for a given period" (Varnes, 1984). Risk assessments result from the interaction between the hazard, the vulnerability of the exposed elements, and the potential damage resulting from a natural phenomenon (Hungr et al., 2001). As a subsequent step to susceptibility analysis, hazard mapping aims to identify the spatial and temporal probability of the occurrence of mass movements, as well as to estimate their trajectory and magnitude (Corominas et al., 2013).

Regarding the identification of potential mass movement trajectories, empirical (geomorphological and geometric) and rational (discrete or continuous) methods can be applied. Discrete rational methods have been developed for mass movements that move individually (e.g., rockfalls) and can be based on simplified geometries of the moving bodies (Agliardi; Crosta, 2003) or in the rigid body ballistics (Azzoni; Barbera; Zaninetti, 1995; Dorren; Kühne, 2016). Continuous rational methods, on the other hand, vary in the complexity of simulating the displacement mechanisms of mass movements, and may include: a) Three-dimensional models based on mixture theory that simulate all phases of matter that make up the material (solid, liquid, and gas) using systems of mathematical equations for fluid mixtures; b) Three-dimensional velocity-pressure models that analyze variations in pore pressure and velocity along the trajectory; and c) Two-dimensional models using depth approximation,

which assume hydrostatic pressure and estimate mass displacement along channels from depth sequences simulations (McDougall, 2017; Rickenmann, 2007).

Stochastic methods can also be employed to examine the trajectory of mass movements (Gruber & Mergili, 2013; Mergili, Krenn & Chu, 2015; Mergili, Schwarz & Kocius, 2019). Such simulations can be combined with physically-based models within a conceptual framework that allows for adaptation to different types of mass movements. In the latter case, the Gravitational Process Path (GPP) model (Wichmann, 2017) can be included. This model simulates trajectories based on stochastic simulations and the propagation of transported material based on simplified physical parameters such as basal friction, mass loss and directional variability. Goetz et al., (2021) and Klade (2022) demonstrated the model's effectiveness by calibrating its parameters for specific geomorphological contexts and obtaining results that were consistent with their field observations.

The GPP model application is restricted in Brazil, especially when it comes to optimization in tropical regions and validation based on mass movement events. This research therefore aimed to assess the shallow landslide hazard in a watershed in the municipality of São Sebastião (SP), which was severely affected by mass movements in 2023, using a physically-based model for trajectory simulation, as well sought to identify buildings in the watershed at risk of landslides.


**Figure 1.** February 2023 event in the municipality of São Sebastião. Source: (a/b) Authors; (c) Fernando Marron/AFP; (d) André Luis Rosa/TV Vanguarda.

## 2. Study Area

The municipality of São Sebastião, located on the northern coast of São Paulo State and approximately 200 km from the state capital, hosts a population of nearly 82,000 inhabitants distributed across 400 km² (IBGE, 2022). The study area comprises the Camburi River watershed, which includes the neighborhood of the same name. Encompassing roughly 37 km², the basin was among the sectors most severely impacted by the extreme rainfall event of February 2023, during which 51 landslide scars were mapped on hillslopes adjacent to densely occupied areas (Figure 2).

In 2018, the Institute for Technological Research (IPT) conducted a risk-sector mapping for the municipality, which identified, within the Camburi neighborhood, housing units situated near cut slopes and natural hillslopes, exhibiting construction patterns ranging from adequate to high quality. The area was subdivided into three sectors,

two of which are associated with the Sol Maior Condominium: one classified as High Risk and another designated as a Monitoring Sector. The third sector was likewise classified as a Monitoring Sector.

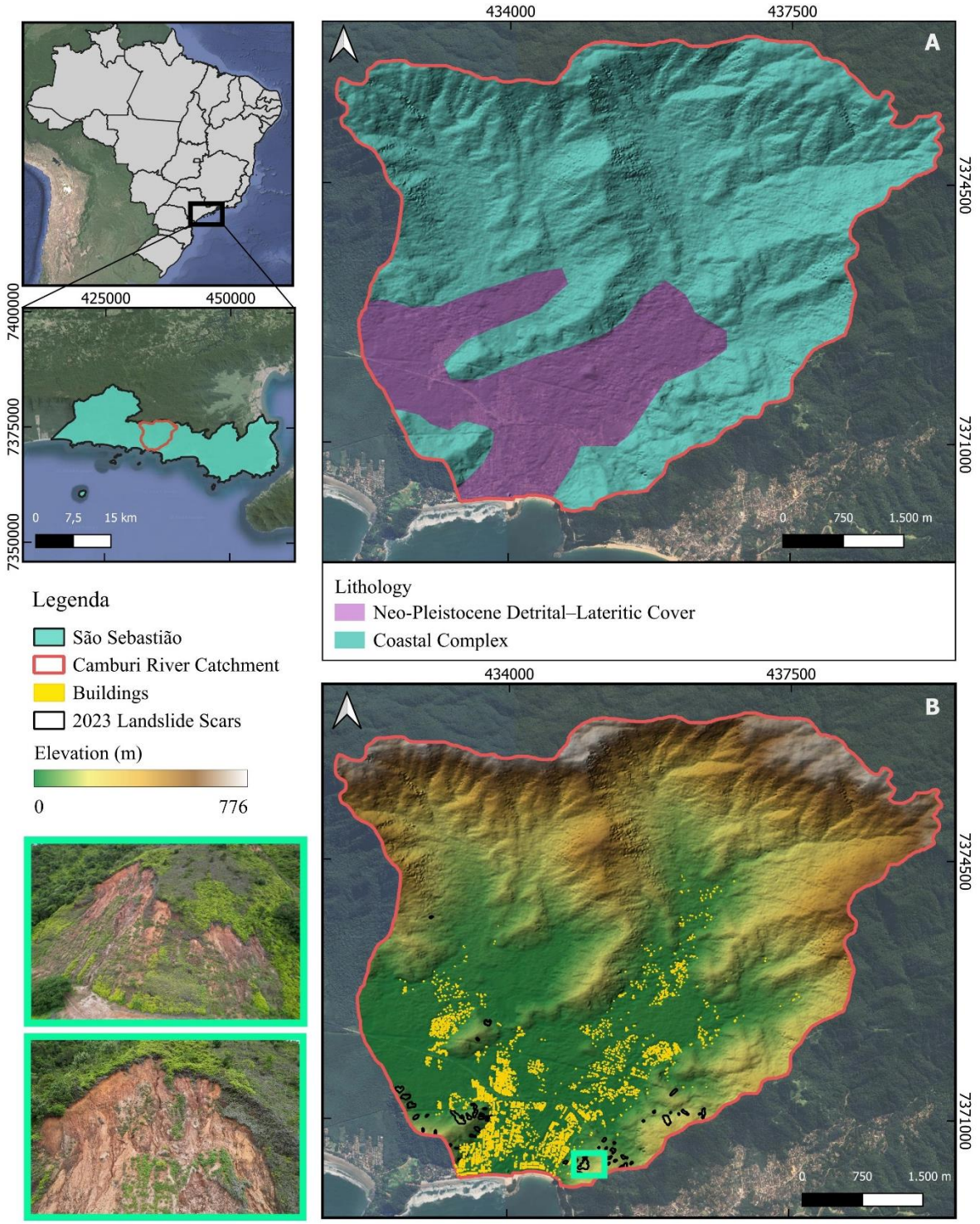


**Figure 2.** Location of the study area. A) Camburi River watershed, indicating the lithostratigraphic units present; B) Hypsometric representation of the basin area, showing the 2023 landslide scars and the residential structures within the affected zone.

The lithostratigraphic units of the basin are divided into two main domains (IBGE, 2023): the coastal complex, dated to the Neoproterozoic Cryogenian and composed of crystalline rocks such as granite, gneiss, and migmatite; and the Upper Pleistocene Quaternary detrital cover. Furthermore, the area can be subdivided into three regional geomorphological compartments—the Serra do Mar, the Coastal Plain, and the Paraitinga Plateau. Pedologically,

the basin is predominantly characterized by aluminic haplic Cambisols with clayey to medium textures (IBGE, 2023).

In São Sebastião, the stretch between Boracéia and Maresias beaches—where the neighborhoods of Sahy and Camburi are located, the most affected by the mass movements that occurred in 2023—stands out for its high rainfall rates, which vary between 1,500 mm and 2,500 mm per year. This coastal strip is the wettest region in the state of São Paulo (Monteiro, 1973), with a significant orographic influence on rainfall distribution (Pellegatti; Galvani, 2010).

## 3. Materials and Methods

### *3.1. Data sources*

Three types of data were used in this research: a) elevation data; b) the location of the 2023 landslide occurrences; and c) land use data and the location of exposed elements. Elevation data were obtained from the TanDEM-X Digital Elevation Model (DEM) (Krieger et al., 2013). The location of the landslides occurred in the 2023 event were derived from the inventory compiled by Bonini et al. (2025). Land use was evaluated with the MapBiomas Collection 2 Beta (10m) (MapBiomas, 2025), and the exposed elements were identified using the OpenStreetMap database.

### *3.2. Susceptibility map*

The physically-based, mathematical model SHALSTAB (*Shallow Landsliding Stability Model*) (Montgomery; Dietrich, 1994) was deployed to assess susceptibility. The model establishes critical daily rainfall thresholds by combining a slope stability model based on the Mohr-Coulomb failure criterion with a steady-state hydrological model, and has been used in several researches in the Serra do Mar (Vieira; Ramos, 2015; Martins et al., 2016; Vieira et al., 2018; Bonini et al., 2020; Pinho; Augusto Filho, 2022).

In this research, susceptibility assessed with the SHALSTAB model relied on minimum and maximum values for the geotechnical and hydrological properties obtained in the literature (Vieira; Ferreira; Gomes, 2015; Wolle, 1988). For each model iteration (1000 iterations), a value for the geotechnical and hydrological properties was selected within the range of the minimum and maximum values (Table 1); the final value of each property is computed by the mean of the selected values across all iterations, resulting in the final susceptibility map.

The SHALSTAB model defines six stability classes. For this research, we considered as unstable the unconditionally unstable class and the class with critical rainfall threshold up to 50 mm/day. Using these classes and the landslide scars identified in the inventory, a confusion matrix was derived to compute the following model accuracy metrics: a) sensitivity (the proportion of correctly classified unstable areas in relation to the total area classified as unstable); b) specificity (the proportion of correctly classified unstable areas in relation to the total area classified as stable; and c) the F1-score (the harmonic mean between model precision and sensitivity). These classes were chosen due to the necessity of establishing their mapping quality level, mainly because these two classes were used as potential shallow landslide release areas for the landslide's runout and velocity estimations in the following step of the methods.

**Table 1**. Geotechnical and hydrological properties used in the susceptibility model iterations

| Geotechnical/hydrological property | Minimum | Maximum | Reference |
|---|---|---|---|
| Soil density (g/cm³) | 1.46 | 1.74 | Wolle (1988) |
| Soil thickness (m) | 0 | 2.5 | Vieira, Ferreira, Gomes (2015) |
| Saturated hydraulic conductivity (m/h) | 0.00036 | 0.36 | |
| Internal friction angle (degrees) | 25 | 37 | |
| Cohesion (MPa) | 0 | 0.011 | |

### 3.3. Runout simulation and hazard mapping

The hazard analysis was performed by estimating the shallow landslides potential trajectories and velocities using the GPP model (Wichmann, 2017), that has in its structure two main modules: the first one used to define the potential trajectories using a Random Walk stochastic method, used in other models for the assessment of mass movements trajectories (Mergili et al., 2015; Mergili; Schwarz; Kociu, 2019); and the second one, to constrain the potential trajectories by simulating friction between the landslide material and the surface. Different friction models are available within the GPP model, given that the model can be used for the simulation of different mass movement types. For shallow landslides simulation, the literature recommends the two-parameter friction model (PCM) (Perla; Chung; McClung, 1980).

In this paper, a two-step full factorial experiment design was used to optimize the GPP modules, following an approach adapted from Goetz et al. (2021). During the first step, the parameter values for the Random Walk simulation were optimized, with an initial experiment to identify the optimal values for each of the three parameters, followed by a second experiment to evaluate the sensibility of the model to small variations of the values of the parameters identified as the most important for the simulation accuracy.

The two parameters of the friction model were optimized during the second step of the optimization process, evaluating all possible parameter value combinations. Both steps of the optimization were carried out in a test area and using parameter ranges obtained from the literature (Goetz et al., 2021; Klade, 2022).

Simulation's adherence to the areas mapped in the landslide inventory was evaluated using the Area Under the Receiver Operating Characteristics curve (AUC-ROC) (Zweig; Campbell, 1993). The optimal parametrization of the coupled two-module model was defined to be the one with the highest value of AUC-ROC. Finally, the landslides trajectories and velocities were computed across the whole study area using this parametrization, considering as release areas for the process initiation the terrains with critical rainfall threshold up to 50 mm/day, as classified by the SHALSTAB model. The hazard map was obtained by classifying the trajectory frequency map into five hazard classes (very low, low, medium, high, and very high), each one of them containing 20% of the simulated trajectories.

**Table 2.** Input data for the optimization of the trajectory and velocity simulations

| | Input data | Value range | Description | Source |
|---|---|---|---|---|
| | DEM | - | Digital Elevation Model | (Krieger et al., 2013) |
| | Release Areas | - | Release areas for process initiation, coded as unique IDs. Rest of the cells classified as No Data. | (Bonini et al., 2025) |
| Random Walk | Slope angle threshold (°) | 20 - 40 | Determines the permissivity for divergent flow simulation | (Wichmann, 2017) |
| | Exponent of divergence (-) | 1.0 - 2.8 | Controls the lateral dispersion of the simulation. | |
| | Persistence factor (-) | 1.0 - 1.5 | Influences the continuity of the landslide trajectory | |
| PCM | Global friction coefficient (μ) (-) | 0.2 - 0.8 | Surface resistance to the flow movement (controls how much the surface friction slows down the process). | |
| | Mass-to-drag ratio (M/D) (m) | 100 - 200 | Flow inertia related to the drag exerted by the mass (controls the tendency of movement persistence | |

### 3.4. Exposed elements

First, the exposed elements were analyzed by considering the land use classes, identified in the MapBiomas database. Next, buildings inside the Camburi basin were defined using OpenStreetMap data, and the location of each building was intersected with the trajectory frequency class. Elements located in areas classified as high and very high hazard were considered threatened.

## 4. Results

### 4.1. Landslide Susceptibility Modeling

The susceptibility model demonstrated satisfactory performance in identifying the landslides recorded in the inventory, achieving a sensitivity of 0.865, a specificity of 0.457, and an F1 score of 0.720. This outcome is likely linked to the sampling iterations incorporated into the model, which account for the minimum and maximum values of geotechnical and hydrological parameters, allowing them to vary within a defined range informed by the specialized literature. The maximum critical rainfall threshold for the initiation of shallow landslides estimated by SHALSTAB reached 218 mm/day, with no cells falling within threshold classes exceeding 400 mm/day (Figure 3). Approximately 35% of the basin area was classified as unconditionally stable, whereas 24% was identified as unconditionally unstable (Figure 4). Thresholds between 0 and 50 mm/day predominate (31% of the area), while nearly 6% of the basin exhibits thresholds between 50 and 100 mm/day, 3% between 100 and 200 mm/day, and only 0.15% between 200 and 400 mm/day.

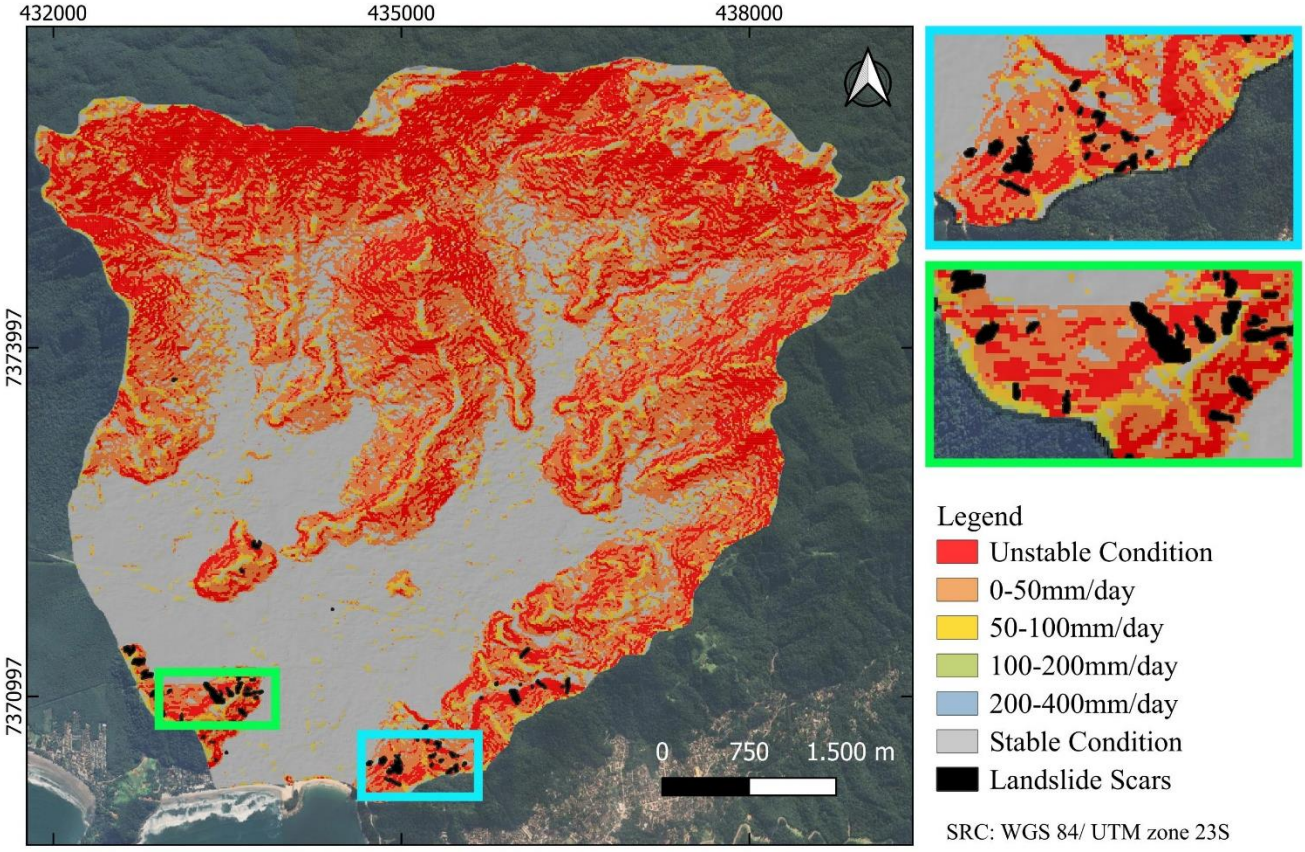


**Figure 3.** Landslide susceptibility map of the Camburi River basin.

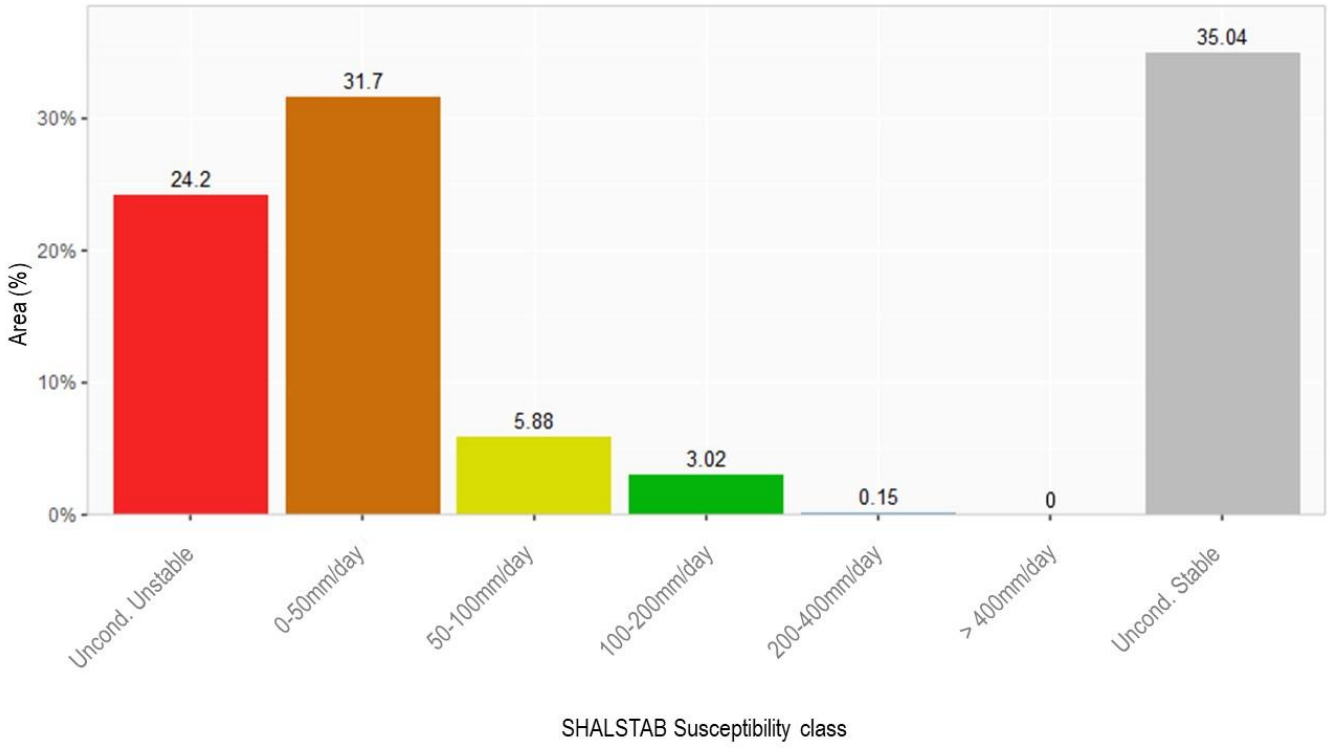


**Figure 4.** Distribution of landslide susceptibility classes within the basin.

*4.2. Runout Simulation*

During the GPP optimization, a total of 102 parameter combinations were generated for the potential-trajectory module. Initially, 90 unique parameter sets were produced. This first experiment revealed a stronger sensitivity to variations in the angle threshold and the exponent of divergence, with the persistence factor exerting comparatively less influence (Figure 5a). The lowest AUC-ROC values (i.e., below 0.500) were associated with angle-threshold values under 30°, whereas the best model performances were obtained for thresholds of 35° (AUC-ROC = 0.604) and 40° (AUC-ROC = 0.628) (Figure 5a). Regarding the exponent of divergence, the first experiment did not allow its individual influence to be clearly distinguished. Consequently, in the second optimization phase of the potential-trajectory module, the angle threshold was restricted to the range that had produced the strongest results (35–40°), while the exponent of divergence was tested between 1.0 and 2.0 in increments of 0.2, with the persistence factor held constant at 1.5. This generated twelve additional parameter combinations (Figure 5b). The outcomes of this procedure pointed to optimal values of 35° for the angle threshold and 1.0 for the exponent of divergence (AUC-ROC = 0.854).

For the optimization of the second GPP module, which corresponds to the PCM friction model, 42 unique parameter combinations were tested (Figure 5c), yielding AUC-ROC values ranging from 0.465 to 0.720. The results indicate that the PCM exhibits greater sensitivity to the friction coefficient than to the mass-to-drag ratio (Figure 5c). The best performance was achieved with a friction coefficient of 0.20 and a mass-to-drag ratio of 180. Using the optimized parameters (Table 3), potential landslide trajectories were then simulated for initiation areas associated with cells exhibiting critical rainfall thresholds equal to or below 50 mm/day (Figure 3).

**Table 3.** Optimized GPP parameter values.

| GPP Module | Parameter | Optimized Value |
|---|---|---|
| Potential Trajectories | Slope-angle threshold | 35° |
| | Exponent of divergence | 1 |
| | Persistence factor | 1.5 |
| PCM Friction Model | Friction coefficient | 0.2 |
| | Mass-to-drag ratio | 180 |

Maximum velocities along the simulated trajectories ranged from zero (in areas not intersected by any simulation) to 32 m/s, with a mean of 11 m/s and a standard deviation of 8.0 m/s. The highest velocities — thus representing the greatest destructive potential — were concentrated on steep upper hillslopes associated with landslide source zones, whereas terminal velocities were observed near or directly within valley bottoms (Figure 6). The area–frequency distribution of simulated trajectories showed an inverse relationship with flow-path convergence (Figure 7). Approximately 92% of the basin is intersected by fewer than 50% of the potential trajectories, while areas affected by more than 80% of possible trajectories account for less than 1% of the total basin area. These highly impacted zones are primarily associated with initiation areas on steep and moderately steep hillslopes, as well as valley-bottom sectors where displaced material tends to accumulate.

The final hazard map, based on the frequency of trajectories, shows that 40% of the basin area is classified as low hazard, followed by 29% and 22% in the very low and moderate hazard classes, respectively. High hazard covers 6% of the basin area, while very high hazard covers only 2%.

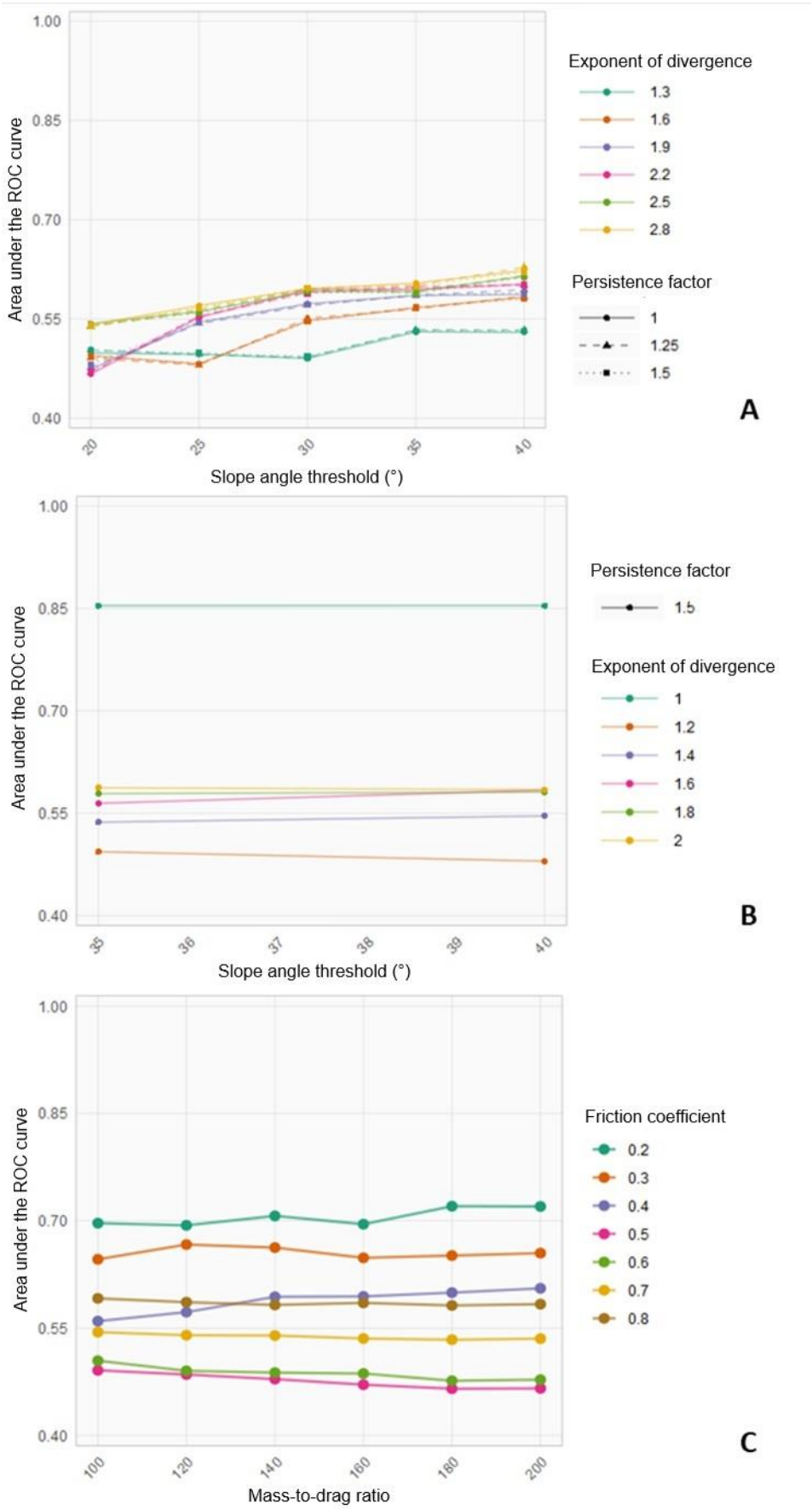


**Figure 5.** (a–b) Variation in AUC-ROC for the Random Walks module; (c) variation in AUC-ROC for the PCM module.

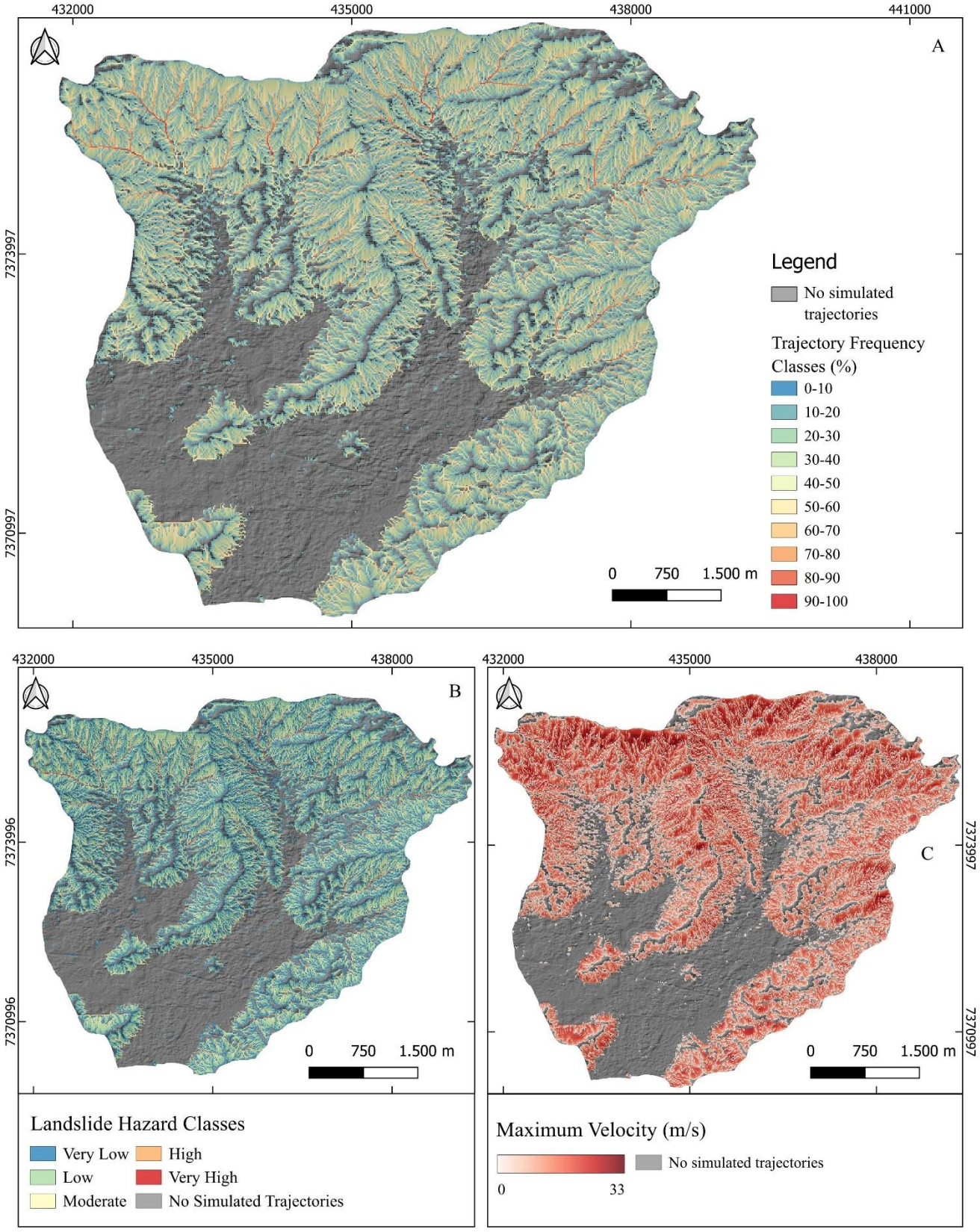


**Figure 6.** (a) Normalized and reclassified trajectory frequency; (b) classified hazard map; (c) maximum velocity along simulated trajectories.

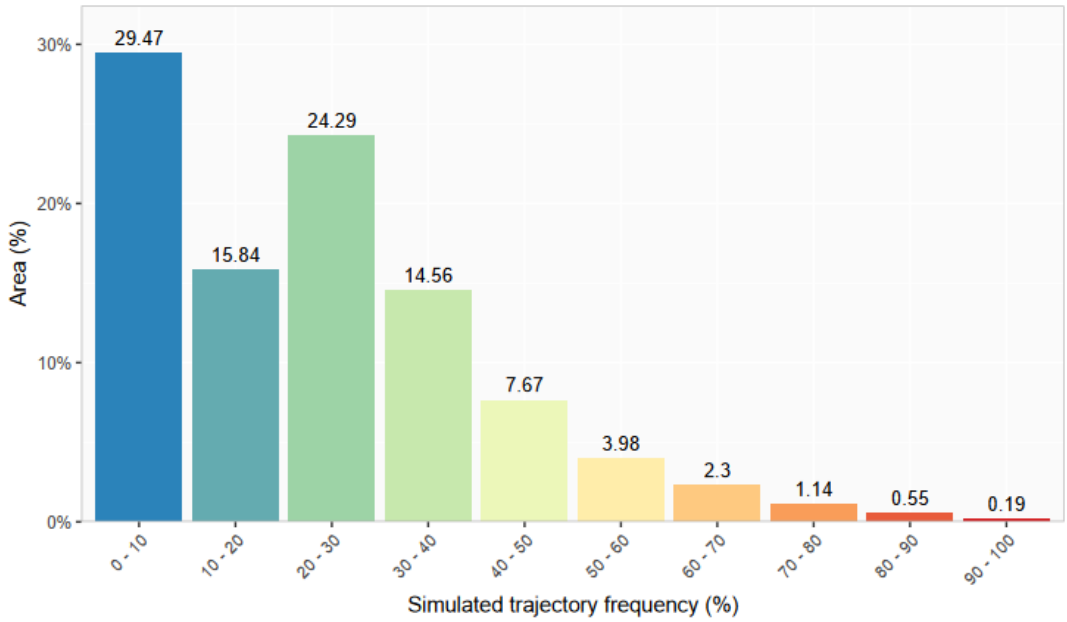


**Figure 7.** Area occupied by each class of the simulated trajectory-frequency map.

*4.3. Exposed Elements*

In terms of land use, the Forest Formation class occupies the largest share of the Camburi Basin, covering approximately 76% of its area and occurring predominantly along the steep hillslopes of the Serra do Mar and the Paraitinga Plateau. The wooded sandbank vegetation, Urban Area, and Mosaic of Uses classes constitute substantial portions of the Coastal Plain, accounting for 15.8%, 4.9%, and 2.56% of the basin area, respectively. All remaining classes together cover less than 0.3% of the Camburi Basin. With respect to exposed elements, a total of 3,667 structures were identified within the basin, concentrated mainly in the Coastal Plain (91%) and, to a lesser extent, along the Serra do Mar hillslopes (9%).

The susceptibility results indicate that the most prone areas are located primarily within the Forest Formation class (Figure 9). A similar pattern is observed for the hazard classes — ranging from very low to very high — which also occur most frequently within this same land-use category. In contrast, the wooded sandbank vegetation, Urban Area, and Mosaic of Uses classes are predominantly associated with the unconditionally stable susceptibility class. With respect to hazard, these land-use categories are mostly situated in areas classified as no hazard, meaning sectors not intersected by any of the simulated trajectories.

With regard to the built structures, the vast majority are located within areas classified as unconditionally stable (94.4%), while only 1.28% (47 structures) fall within zones mapped as unconditionally unstable. In the susceptibility class with thresholds up to 50 mm/day, 113 structures were identified (3.08%), whereas the 50–100 mm/day and 100–200 mm/day classes contain only 0.9% (33) and 0.33% (12) of the structures, respectively (Figure 8).

Similarly, approximately 89.4% of the area occupied by the structures lies within the no-hazard zone. However, 3.12% of the building area falls within the very-low hazard class, 4.53% within the low hazard class, and 2.38% within the moderate hazard class. Only 0.57% of the total building area corresponds to the high (0.55%) and very high (0.02%) hazard classes. It is important to note that a single structure may span areas associated with different hazard levels.

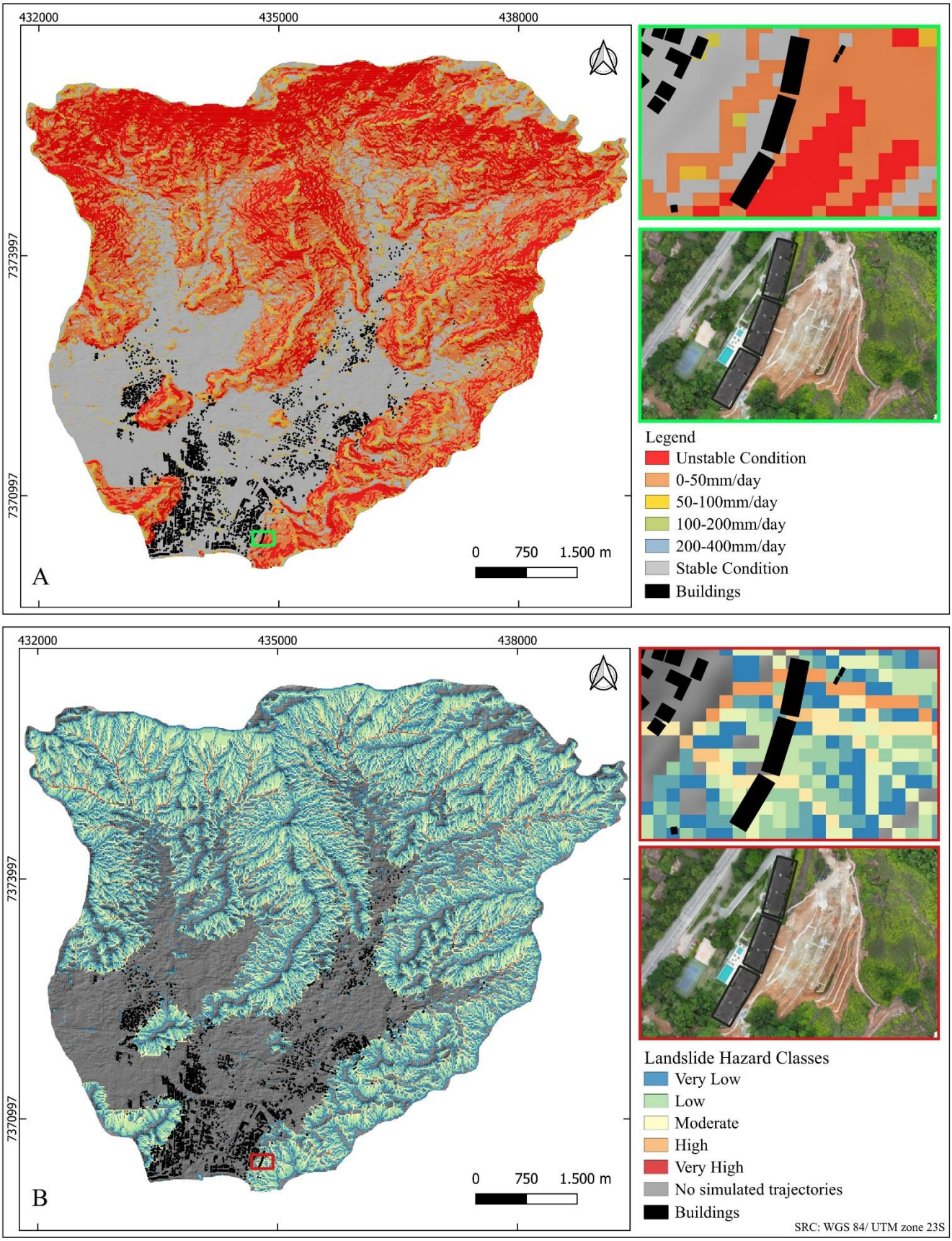


**Figure** 8. (a) Susceptibility classes and structures; (b) hazard classes and structures.

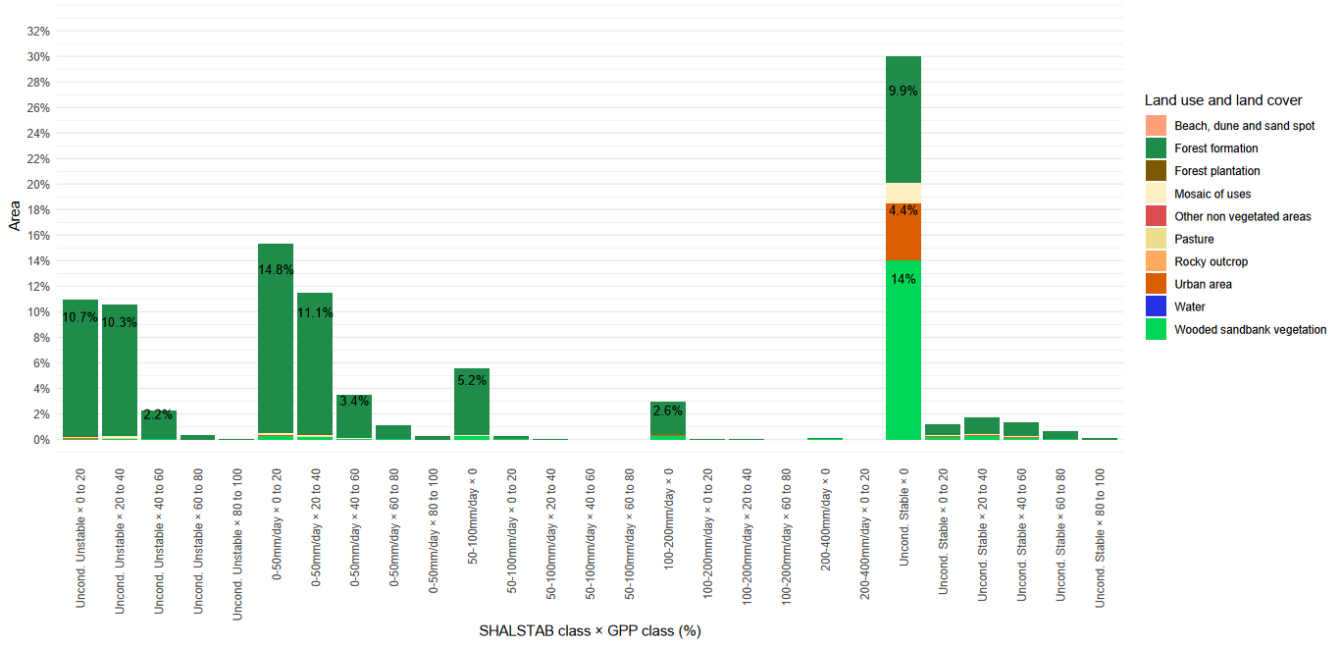


**Figure 9.** SHALSTAB classes and trajectory-frequency classes in relation to land use.

## 5. Discussion

### *5.1 Shalstab*

The model was deemed satisfactory in identifying areas susceptible to landslides, despite its lower specificity, which indicates a substantial number of false positives—that is, stable areas incorrectly classified as unstable. This result, however, is understandable given that the mapped scars are concentrated in the southern portion of the basin and occupy a very small area relative to the total extent evaluated by the model. Even so, the F1 score reflects a balanced trade-off between precision and recall, reinforcing the model's usefulness for susceptibility mapping.

The low cohesion values, as previously demonstrated by Guimarães (2000), reinforce the predominant role of topographic control in the triggering of landslides. Because no spatially distributed data on soil properties were available, simplifying the model by assuming near-zero cohesion proved methodologically more appropriate, allowing SHALSTAB, whose formulation inherently emphasizes topographic control, to operate more efficiently. In contrast, the friction angles used were relatively high on average, which helped constrain the overestimation of unstable areas. The saturated hydraulic conductivity values reflect the challenges posed by the high spatial variability of this parameter, largely due to the absence of spatially distributed measurements and to the presence of hydraulic discontinuities at critical depths (between 1 m and 2.5 m) (Vieira, Ferreira, & Gomes, 2015). Soil depth exhibited little variation among the tested parameters, a pattern that can be attributed to the predominance of Cambisols within the basin.

The areas classified as unconditionally unstable are concentrated mainly along the upper hillslopes of the Serra do Mar, at elevations above 400 meters, where steep gradients predominate and land cover is dominated by forest formations. These sectors also coincide with the occurrence of Cambisols, which are shallow and poorly developed soils whose characteristics promote rapid water infiltration and, consequently, increase hillslope instability. The susceptibility zones located closer to inhabited areas are associated with critical rainfall thresholds of up to 100 mm per day, extend for roughly 200 meters, and occur mostly on Cambisols.

One of the main limitations of the model concerns the definition of susceptibility classes based on rainfall thresholds. In this study, a large portion of the basin was classified as susceptible under rainfall events of up to 50 mm per day. However, because annual precipitation in the area can reach 2,500 mm, events of this magnitude occur frequently throughout the year and do not necessarily result in landslides. Previous studies in the Serra do Mar have already highlighted this tendency to overestimate unstable areas, which is largely explained by the fact that SHALSTAB models the potential for instability under idealized and generalized conditions that depend heavily on topography and incorporate simplified hydrological assumptions (Bonini et al., 2020; Guimarães, 2000;

Vieira et al., 2018; Vieira and Ramos, 2015). Model accuracy is also constrained by the limited availability of detailed, spatially distributed data on soil properties, vegetation cover, and local hydrological dynamics. Even so, given the need to incorporate rainfall values into hazard modeling, the approach adopted here proved more suitable than alternative methods that rely on long historical rainfall series, which are not always available.

### *5.2. Gravitational Process Path – GPP*

The persistence factor governs how closely a simulated trajectory follows its previous direction, effectively representing the inertia of the moving material. Given its limited variation across the simulations, the results suggest that the modeled paths tend to follow relatively continuous trajectories with few abrupt changes in direction, especially because they traverse the steep hillslopes of the Serra do Mar, where terrain geometry strongly constrains movement. The slope-angle threshold determines the extent to which the flow path can deviate laterally, thereby allowing or restricting areas of greater lateral spreading. The higher AUC-ROC values obtained for steeper angle thresholds indicate that the trajectories do not necessarily follow the cell with the lowest local gradient; instead, they spread laterally with some frequency, consequently enlarging the affected area. In light of these results, the exponent of divergence, which controls the likelihood of lateral spreading, particularly in gentler terrain, reached a lower optimal value that balances the higher angle-threshold parameter (Wichmann, 2017).

The friction coefficient, which plays a central role in shaping process behavior along the simulated paths, determines where the moving material comes to rest and deposition begins. The optimal value obtained was 0.2, which is close to that suggested by Wichmann (2017) for agricultural areas. This result is consistent with the mapped scars, as many of them are located in zones classified as mosaics of land use. This discontinuous land cover, combined with the presence of shallow cambisols and steep slopes, facilitates downslope movement and contributes to longer runout distances. The mass-to-drag ratio mainly influences velocity along the steeper portions of the path. However, this parameter exerts limited control on the trajectory calculations, which can be attributed to the well-known uniqueness problem associated with this ratio. Different combinations of μ and M/D can produce the same runout distance, introducing mathematical redundancy into the model (Perla, Cheng, and McClung, 1980).

It is important to note that the trajectories simulated by the GPP model are generated from a prior landslide susceptibility map, which defines the rupture areas. Because shallow landslides tend to exhibit relatively short runout distances compared with debris flows, the paths simulated by the GPP remain largely confined to the zones previously classified as unstable by the susceptibility model. Consequently, the effectiveness of the GPP is directly conditioned by the quality and accuracy of the input model.

### *5.3. Exposed Elements*

Approximately 77 percent of the structures are located in areas classified as urbanized, which correspond to places with human occupation and built surfaces, that is, areas identified as impervious by the MapBiomas land-cover mapping. The Serra do Mar is predominantly covered by areas classified as Forest Formation and contains several conservation units and legally protected areas, including the Serra do Mar State Park, Atlantic Forest Reserves, and Permanent Preservation Areas (APPs), all situated on steep terrain. These legal restrictions are intended to prevent settlement in environmentally sensitive regions. It is important to note that these steep areas also coincide with zones of higher landslide susceptibility. In this context, at least 160 structures were identified within zones classified as unconditionally unstable, even under rainfall conditions below 50 mm per day.

Regarding the hazard, roughly 5% of the structures lie within sectors showing some indication of hazard, although fewer than 1% are located in areas classified as high or very high hazard. This pattern suggests that buildings tend to be affected by specific landslide trajectories rather than by all potential rupture zones. Even so, despite the low frequency of simulated trajectories, structures may still be impacted by sporadic events that carry a high potential for damage.

Although most buildings are situated within zones classified as no hazard or low hazard, chiefly on the coastal plain, it is important to emphasize that extreme events often lead to complex mass-movement processes. In such cases, landslides may transition into debris or mud flows, substantially increasing the affected area. This study did not include the modeling or analysis of such flow processes, which represents a limitation in the comprehensive assessment of hazard conditions.

A comparison between susceptibility classes and the risk sectors mapped by the IPT in 2018 for the Camburi watershed shows that Sector 1, classified as R3, is identified by SHALSTAB as unconditionally unstable, as is Sector 2, which is designated as a monitoring sector. Sector 3, also classified as a monitoring sector, falls within the instability class associated with rainfall thresholds of up to 50 mm per day for landslide triggering. Regarding hazard, the sectors mapped by the IPT are situated within areas classified as low to moderate hazard, although other areas classified as high hazard were not formally designated as risk sectors by the agency.

## 6. Conclusions

Landslides are natural processes that become hazards when they occur in areas near human settlements, which underscores the importance of tools capable of mapping susceptibility and hazard in order to guide preventive measures. In this study, the models applied for susceptibility and hazard analysis were considered satisfactory. It is important to emphasize, however, that these models are subject to significant limitations due to the lack of spatially distributed hydrological and geotechnical data, which reduces their overall effectiveness. Moreover, the study demonstrated the feasibility of calibrating models through statistical procedures, highlighting the practicality of this approach for defining optimal parameters in models that are still seldom used in Brazil, such as the Gravitational Process Path.

With respect to the exposed elements, although the difference is subtle, the hazard level associated with the structures is higher than their susceptibility, indicating that the runout of the landslides exerts a more significant influence than the location of their initiation. The relatively small number of exposed elements can be partly attributed to the fact that the model calibration was specifically oriented toward predicting the runout of shallow landslides. Nevertheless, during extreme events, cascading processes are common, in which initial landslides may trigger subsequent debris flows.

The workflow implemented in this study and the results obtained can support future hazard assessments in the municipality of São Sebastião and in other areas of the Serra do Mar. In addition, the analysis of exposed elements may assist in the development of preventive measures for the Camburi River basin.

**Authors contributions:** Concept and methodology: S.B.C., B.C.V., and J.E.B.; data collection and formal analysis: S.B.C., M.T.S.O., and J.E.B.; manuscript writing: S.B.C.; writing and revision: M.T.S.O., J.E.B., T.D.M., and B.C.V.; critical revision: M.T.S.O., J.E.B., T.D.M., and B.C.V.; final approval of the manuscript: all authors. All authors read and agreed to the final version of the manuscript.

**Funding:** This research was funded by CNPq, through resources granted by Chamada Universal (Processes: 409314/2023-4; 305371/2023-1); by the São Paulo Research Foundation (FAPESP) (Processes: #2021/04621-6, #2024/01662-1, and #2022/0132-6); and by the Graduate Program in Physical Geography at the University of São Paulo (PPGF).

**Acknowledgments:** We would like to thank the reviewers of this article for their contributions; the Civil Defense of São Sebastião for technical and logistical support during fieldwork; and the Department of Geography at the University of São Paulo.

**Conflict of interest:** The authors declare that there is no conflict of interest.

## References

1. AGLIARDI, F; CROSTA, G. B. High resolution three-dimensional numerical modelling of rockfalls. International Journal of Rock Mechanics and Mining Sciences, vol. 40, no 4, p. 455–471, 2003.
2. ALCÁNTARA-AYALA, Irasema. Landslides in a changing world. Landslides, 15 jan. 2025. DOI: 10.1007/s10346-024-02451-1.
3. AVELAR, André S.; NETTO, Ana L. Coelho; LACERDA, Willy A.; BECKER, Leonardo B.; MENDONÇA, Marcos B. Mechanisms of the Recent Catastrophic Landslides in the Mountainous Range of Rio de Janeiro, Brazil. Landslide Science and Practice. Berlin, Heidelberg: Springer Berlin Heidelberg, 2013. p. 265–270. DOI: 10.1007/978-3-642-31337-0_34.

4. AZZONI, A; BARBERA, G. L; ZANINETTI, A. Analysis and prediction of rockfalls using a mathematical model. International Journal of Rock Mechanics and Mining Science. International Journal of Rock Mechanics and Mining Science, vol. 32, p. 709–724, 1995.
5. BONINI, José Eduardo; BATEIRA, Carlos Valdir de Meneses; DIAS, Vivian Cristina; MARTINS, Tiago Damas; VIEIRA, Bianca Carvalho. Suscetibilidade a escorregamentos rasos a partir de parâmetros morfométricos e dos modelos SHALSTAB e do Valor Informativo. Confins, vol. 46, 2020. DOI:10.4000/confins.30323.
6. BONINI, José Eduardo; SANCHES ROSS, Jurandyr Luciano; MARTINS, Tiago D.; VIEIRA, Bianca Carvalho. Escorregamentos rasos em São Luiz do Paraitinga (SP, Brasil) (2009-2010). Physis Terrae - Revista Ibero-Afro-Americana de Geografia Física e Ambiente, vol. 2, no 2, p. 85–99, 27 jan. 2021. DOI:10.21814/physisterrae.3076.
7. BONINI, José Eduardo; MARTINS, Tiago Damas; SUGIYAMA, Marina Tamaki de Oliveira; VIEIRA, Bianca Carvalho. Landslide inventory of the 2023 Serra do Mar disaster (Brazil). Discover Geoscience 2025 3:1, vol. 3, no 1, p. 1–17, 22 abr. 2025. DOI 10.1007/S44288-025-00153-2. Disponível em: https://link.springer.com/article/10.1007/s44288-025-00153-2. Acessado em: 28 abr. 2025.
8. BONINI, José Eduardo; VIEIRA, Bianca Carvalho; MARTINS, Tiago Damas. Semiautomatic inventory and geomorphological characterization of mass movements using high-resolution images and open-source software in the Ribeira de Iguape Valley, Brazil. Journal of South American Earth Sciences, vol. 119, p. 104029, nov. 2022. DOI: 10.1016/j.jsames.2022.104029.
9. CONRAD, O.; BECHTEL, B.; BOCK, M.; DIETRICH, H.; FISCHER, E.; GERLITZ, L.; WEHBERG, J.; WICHMANN, V.; BÖHNER, J. System for Automated Geoscientific Analyses (SAGA) v. 2.1.4. Geoscientific Model Development, vol. 8, no 7, p. 1991–2007, 7 jul. 2015. DOI: 10.5194/gmd-8-1991-2015.
10. COROMINAS, J.; VAN WESTEN, C.; FRATTINI, P.; CASCINI, L.; MALET, J.-P.; FOTOPOULOU, S.; CATANI, F.; VAN DEN EECKHAUT, M.; MAVROULI, O.; AGLIARDI, F.; PITILAKIS, K.; WINTER, M. G.; PASTOR, M.; FERLISI, S.; TOFANI, V.; HERVÁS, J.; SMITH, J. T. Recommendations for the quantitative analysis of landslide risk. Bulletin of Engineering Geology and the Environment, 24 nov. 2013. DOI:10.1007/s10064-013-0538-8.
11. DO PINHO, Thiago Machado; AUGUSTO FILHO, Oswaldo. Landslide susceptibility mapping using the infinite slope, SHALSTAB, SINMAP, and TRIGRS models in Serra do Mar, Brazil. **Journal of Mountain Science**, vol. 19, nº 4, p. 1018–1036, 13 abr. 2022. DOI:10.1007/s11629-021-7057-z.
12. CPRM - GEOLOGICAL SURVEY OF BRAZIL. Maps of Susceptibility to Gravitational Movements 1:25,000. Explanatory Technical Note. Bitar, OY (Org), 2017.
13. DORREN, L; KÜHNE, R. Comparing the 3D rockfall simulation models Rockyfor3D and RAMMS: ROCKFALL at a case study site in Switzerland. INTERPRAEVENT 2016 – Extended Abstracts, p. 2–3, 2016.
14. FERNANDES, Nelson F.; GUIMARÃES, Renato F.; GOMES, Roberto A.T.; VIEIRA, Bianca C.; MONTGOMERY, David R.; GREENBERG, Harvey. Topographic controls of landslides in Rio de Janeiro: field evidence and modeling. CATENA, vol. 55, no 2, p. 163–181, jan. 2004. DOI:10.1016/S0341-8162(03)00115-2.
15. G1. Temporal devastador no litoral norte de SP completa um mês. 2023. Disponível em: https://g1.globo.com/sp/vale-do-paraiba-regiao/noticia/2023/03/19/temporal-devastador-no-litoral-norte-de-sp-completa-um-mes-confira-um-resumo-da-tragedia.ghtml. Acessado em: 19 mar. 2025.
16. GOETZ, Jason; KOHRS, Robin; PARRA HORMAZÁBAL, Eric; BUSTOS MORALES, Manuel; ARANEDA RIQUELME, María Belén; HENRÍQUEZ, Cristián; BRENNING, Alexander. Optimizing and validating the Gravitational Process Path model for regional debris-flow runout modelling. Natural Hazards and Earth System Sciences, vol. 21, no 8, p. 2543–2562, 25 ago. 2021. DOI:10.5194/nhess-21-2543-2021.
17. GOMES, Roberto A. T.; GUIMARÃES, Renato F.; CARVALHO, Osmar A.; FERNANDES, Nelson F.; VARGAS, Eurípedes A.; MARTINS, Éder S. Identification of the affected areas by mass movement through a physically based model of

landslide hazard combined with an empirical model of debris flow. Natural Hazards, vol. 45, no 2, p. 197, 1 maio 2008. DOI:10.1007/s11069-007-9160-z.

18. GÓMEZ, Derly; GARCÍA, Edwin F.; ARISTIZÁBAL, Edier. Spatial and temporal landslide distributions using global and open landslide databases. Natural Hazards, vol. 117, no 1, p. 25–55, 1 maio 2023. DOI:10.1007/s11069-023-05848-8.
19. GRUBER, F. E.; MERGILI, M. Regional-scale analysis of high-mountain multi-hazard and risk indicators in the Pamir (Tajikistan) with GRASS GIS. Natural Hazards and Earth System Sciences, vol. 13, no 11, p. 2779–2796, 7 nov. 2013. DOI: 10.5194/nhess-13-2779-2013.
20. GUIMARÃES, R. F. Utilização de um Modelo de Previsão de Áreas Susceptíveis a Escorregamentos Rasos com Controle Topográfico: Adequação e Calibração em Duas Bacias de Drenagem. 2000. 327 f. Tese de Doutorado – UFRJ, Rio de Janeiro, 2000.
21. GUIMARÃES, Renato Fontes; MONTGOMERY, David R.; GREENBERG, Harvey M.; FERNANDES, Nelson Ferreira; TRANCOSO GOMES, Roberto Arnaldo; DE CARVALHO, Osmar Abílio. Parameterization of soil properties for a model of topographic controls on shallow landsliding: application to Rio de Janeiro. Engineering Geology, vol. 69, no 1–2, p. 99–108, abr. 2003. DOI:10.1016/S0013-7952(02)00263-6.
22. HUNGR, Oldrich; EVANS, S. G.; BOVIS, M. J.; HUTCHINSON, J. N. A review of the classification of landslides of the flow type. Environmental and Engineering Geoscience, vol. 7, no 3, p. 221–238, 1 ago. 2001. DOI: 10.2113/gseegeosci.7.3.221.
23. IBGE. Censo de 2022. 2022. IBGE - Instituto Brasileiro de Geografia e Estatística. Disponível em: https://censo2022.ibge.gov.br/panorama/?utm_source=ibge&utm_medium=home&utm_campaign=portal. Acessado em: 13 jan. 2024.
24. IBGE. Mapa geológico do Brasil. 2023. Disponível em: https://www.ibge.gov.br/geociencias/informacoes-ambientais/pedologia/10871-pedologia.html?=&t=downloads. Acessado em: 19 jan. 2024.
25. IBGE. Mapa pedológico do Brasil. 2023. Disponível em: https://www.ibge.gov.br/geociencias/informacoes-ambientais/pedologia/10871-pedologia.html?=&t=downloads. Acessado em: 19 jan. 2024.
26. IPT. Mapeamento de áreas de risco de movimentos de massa no município de São Sebastião, SP. Instituto de Pesquisas Tecnológicas, 2018.
27. IPT - INSTITUTE OF TECHNICAL RESEARCH OF THE STATE OF SÃO PAULO; CPRM - GEOLOGICAL SURVEY OF BRAZIL. Maps of Susceptibility to Gravitational Movements 1:25,000. Explanatory Technical Note, Bitar, OY (Org), p. 53, 2014.
28. JONES, Fred O. Landslides of Rio de Janeiro and the Serra das Araras escarpment, Brazil. [S. l.: s. n.], 1973. DOI: 10.3133/pp697.
29. KANJI, Milton A.; CRUZ, Paulo T.; MASSAD, Faiçal. Debris flow affecting the Cubatão Oil Refinery, Brazil. Landslides, vol. 5, no 1, p. 71–82, 28 fev. 2008. DOI: 10.1007/s10346-007-0110-3.
30. KLADE, Martina. Reichweitenmodellierung von flachgründigen Hangrutschungen mit dem Gravitational Process Path Model in ausgewählten Gemeinden des Steirischen Beckens. 2022. Masterarbeit – Universität Graz, 2022.
31. KRIEGER, Gerhard; ZINK, Manfred; BACHMANN, Markus; BRÄUTIGAM, Benjamin; SCHULZE, Daniel; MARTONE, Michele; RIZZOLI, Paola; STEINBRECHER, Ulrich; WALTER ANTONY, John; DE ZAN, Francesco; HAJNSEK, Irena; PAPATHANASSIOU, Kostas; KUGLER, Florian; RODRIGUEZ CASSOLA, Marc; YOUNIS, Marwan; BAUMGARTNER, Stefan; LÓPEZ-DEKKER, Paco; PRATS, Pau; MOREIRA, Alberto. TanDEM-X: A radar interferometer with two formation-flying satellites. **Acta Astronautica**, vol. 89, p. 83–98, ago. 2013. DOI: 10.1016/j.actaastro.2013.03.008.
32. MAPBIOMAS. Coleção 2 (beta) de Mapas Anuais de Cobertura e Uso da Terra do Brasil com 10 metros de resolução espacial. Disponível em: https://storage.googleapis.com/mapbiomas-

public/initiatives/brasil/lulc_10m/collection_2/integration/mapbiomas_10m_collection2_integration_v1-classification_2023.tif. Acessado em: 14 fev. 2025.

33. MARENGO, Jose A.; CUNHA, Ana P.; SELUCHI, Marcelo E.; CAMARINHA, Pedro I.; DOLIF, Giovanni; SPERLING, Vinicius B.; ALCÂNTARA, Enner H.; RAMOS, Andrea M.; ANDRADE, Marcio M.; STABILE, Rodrigo A.; MANTOVANI, José; PARK, Edward; ALVALA, Regina C.; MORAES, Osvaldo L.; NOBRE, Carlos A.; GONCALVES, Demerval. Heavy rains and hydrogeological disasters on February 18th–19th, 2023, in the city of São Sebastião, São Paulo, Brazil: from meteorological causes to early warnings. Natural Hazards, vol. 120, no 8, p. 7997–8024, 28 jun. 2024. DOI: 10.1007/s11069-024-06558-5.
34. MARTINS, T; OKA-FIORI, C; VIEIRA, B; MONTGOMERY, D. Assessment of Lidar-derived DTMs for landslide susceptibility mapping: Application in the Brazilian subtropical forest. Landslides and Engineered Slopes. Experience, Theory and Practice. [S. l.]: CRC Press, 2016. p. 1389–1392. DOI: 10.1201/b21520-170.
35. MARTINS, Tiago Damas; VIEIRA, Bianca Carvalho; FERNANDES, Nelson Ferreira; OKAFIORI, Chisato; MONTGOMERY, David R. Application of the SHALSTAB model for the identification of areas susceptible to landslides: Brazilian case studies. Revista de Geomorfologie, vol. 19, no 1, p. 136–144, 30 dez. 2017. DOI: 10.21094/rg.2017.015.
36. MCDOUGALL, Scott. 2014 Canadian Geotechnical Colloquium: Landslide runout analysis — current practice and challenges. Canadian Geotechnical Journal, vol. 54, no 5, p. 605–620, maio 2017. DOI: 10.1139/cgj-2016-0104.
37. MEIS, M.R.M; SIL. J.X. Considerações geomorfológicas a propósito dos movimentos de massa ocorridos no Rio de Janeiro. Revista Brasileira de Geomorfologia, vol. 30, no 1, 1968.
38. MERGILI, M.; KRENN, J.; CHU, H.-J. r.randomwalk v1, a multi-functional conceptual tool for mass movement routing. Geoscientific Model Development, vol. 8, no 12, p. 4027–4043, 16 dez. 2015. DOI: 10.5194/gmd-8-4027-2015.
39. MERGILI, Martin; SCHWARZ, Leonhard; KOCIU, Arben. Combining release and runout in statistical landslide susceptibility modeling. Landslides, vol. 16, no 11, p. 2151–2165, 1 nov. 2019. DOI: 10.1007/s10346-019-01222-7.
40. MONTEIRO, Carlos Augusto de Figueiredo. A Dinâmica climática e as chuvas no Estado de São Paulo: estudo geográfico sob forma de atlas. São Paulo: Instituto de Geografia (USP), 1973.
41. MONTGOMERY, David R.; DIETRICH, William E. A physically based model for the topographic control on shallow landsliding. Water Resources Research, vol. 30, no 4, p. 1153–1171, 9 abr. 1994. DOI: 10.1029/93WR02979.
42. O GLOBO. Após tragédia São Sebastião tenta evitar que moradores voltem a áreas de risco. 2023. Disponível em: https://oglobo.globo.com/brasil/noticia/2023/02/apos-tragedia-sao-sebastiao-tenta-evitar-que-moradores-voltem-a-areas-de-risco.ghtml. Acessado em: 21 mar. 2025.
43. PAWLEY S. Rsagacmd: Linking R with the Open-Source "SAGA-GIS" Software. 2024. R package version 0.4.3. Disponível em: https://stevenpawley.github.io/Rsagacmd/. Acessado em: 6 mar. 2025.
44. PELLEGATTI, Cesar Henrique Gonçalves; GALVANI, Emerson. Avaliação da precipitação na Serra do Mar - SP em eventos de diferentes intensidade e duração. GEOUSP: espaço e tempo, no 27, p. 147–148, 2010.
45. PERLA, R.; CHENG, T. T; MCCLUNG, D. M. A two-parameter model of snow-avalanche motion. J. Glaciol., vol. 26, p. 197–207, 1980.
46. R CORE TEAM. R: A language and environment for statistical computing. 2021. R: A language and environment for statistical computing, Vienna, Austria. Disponível em: https://www.R-project.org/. Acessado em: 6 mar. 2025.
47. RICKENMANN, Dieter. Runout prediction methods. Debris-flow Hazards and Related Phenomena. Berlin, Heidelberg: Springer Berlin Heidelberg, [s. d.]. p. 305–324, 2007. DOI: 10.1007/3-540-27129-5_13.
48. VARNES, D.J. Landslide Hazard Zonation: A Review of Principles and Practice. NaturalHazards, vol. Unesco, no Paris, 1984.

49. VIEIRA, Bianca Carvalho; FERNANDES, Nelson Ferreira; AUGUSTO FILHO, Oswaldo; MARTINS, Tiago Damas; MONTGOMERY, David R. Assessing shallow landslide hazards using the TRIGRS and SHALSTAB models, Serra do Mar, Brazil. Environmental Earth Sciences, vol. 77, no 6, p. 260, 27 mar. 2018. DOI: 10.1007/s12665-018-7436-0.
50. VIEIRA, Bianca Carvalho; FERREIRA, Fabiana Souza; GOMES, Maria Carolina Villaça. PROPRIEDADES FÍSICAS E HIDROLÓGICAS DOS SOLOS E OS ESCORREGAMENTOS RASOS NA SERRA DO MAR PAULISTA. Raega - O Espaço Geográfico em Análise, vol. 34, p. 307, 23 set. 2015. DOI: 10.5380/raega.v34i0.40739.
51. VIEIRA, Bianca Carvalho; GRAMANI, Marcelo Fischer. Serra do Mar: The Most "Tormented" Relief in Brazil. In: VIEIRA, Bianca Carvalho; SALGADO, André Augusto Rodrigues; SANTOS, Leonardo José Cordeiro (orgs.). Landscapes and Landforms of Brazil. [S. l.]: Dordrecht: Springer, 2015. p. 285–297.
52. VIEIRA, Bianca Carvalho; MARTINS, Tiago Damas; DA SILVA, Telma Mendes; BONINI, José Eduardo. How far have we come? Review of main public policies to reduce landslide impacts in Brazil. Journal of Mountain Science, vol. 21, no 9, p. 2891–2904, 10 set. 2024. DOI: 10.1007/s11629-024-8898-z.
53. VIEIRA, Bianca Carvalho; RAMOS, Henrique. Aplicação do modelo Shalstab para mapeamento da suscetilidade a escorregamentos rasos em Caraguatatuba, Serra do Mar (SP). Geography Department University of Sao Paulo, vol. 29, p. 161, 17 jun. 2015. DOI: 10.11606/rdg.v29i0.102087.
54. WICHMANN, Volker. The Gravitational Process Path (GPP) model (v1.0) – a GIS-based simulation framework for gravitational processes. Geoscientific Model Development, vol. 10, no 9, p. 3309–3327, 8 set. 2017. DOI: 10.5194/gmd-10-3309-2017.
55. WOLLE, C. M. Análise dos escorregamentos translacionais rasos numa região da Serra do Mar. 1988. 406 f. Tese de Doutorado – Universidade de São Paulo, São Paulo, 1988.
56. ZWEIG, M. H; CAMPBELL, G. Receiver-operating characteristic (ROC) plots: a fundamental evaluation tool in clinical medicine. Clinical Chemistry, vol. 39, no 4, p. 561–577, 1993.